Neuron, Vol. 36, 739–750, November 14, 2002, Copyright ©2002 by Cell Press

Lateral Connectivity and Contextual Interactions in Macaque Primary Visual Cortex

Dan D. Stettler,[1] Aniruddha Das,[1] Jean Bennett,[2] and Charles D. Gilbert[1,3]
[1]The Rockefeller University
1230 York Avenue
New York, New York 10021
[2] Kirby Center for Molecular Ophthalmology
University of Pennsylvania
310 Stellar-Chance
Philadelphia, Pennsylvania 19104

Summary

Two components of cortical circuits could mediate contour integration in primary visual cortex (V1): intrinsic horizontal connections and feedback from higher cortical areas. To distinguish between these, we combined functional mapping with a new technique for labeling axons, a recombinant adenovirus bearing the gene for green fluorescent protein (GFP), to determine the extent, density, and orientation specificity of V1 intrinsic connections and V2 to V1 feedback. Both connections cover portions of V1 representing regions of visual space up to eight times larger than receptive fields as classically defined, though the intrinsic connections are an order of magnitude denser than the feedback. Whereas the intrinsic connections link similarly oriented domains in V1, V2 to V1 feedback displays no such specificity. These findings suggest that V1 intrinsic horizontal connections provide a more likely substrate for contour integration.

Introduction

Neurons in V1 analyze not just the attributes of local features, such as orientation, but also the global characteristics of extended contours. Superficial V1 neurons are sensitive to complex stimuli occupying larger areas than indicated by their responses to simple stimuli, and this sensitivity depends on the geometry of the stimulus components (Nelson and Frost, 1985; Kapadia et al., 1995, 1999, 2000). For example, a V1 neuron's response to a bar in the center of its receptive field (RF) can be facilitated by a flanking iso-oriented, colinear bar that does not elicit a response if presented alone (Kapadia et al., 1995, 1999). Human observers exhibit a comparable increased ability to detect a dim bar in the presence of a flank, and the geometric constraints limiting such facilitation in both V1 neuronal and human performance are identical. It has been proposed that V1 selectivity to such stimuli is mediated by long-range horizontal connections intrinsic to V1 (Gilbert and Wiesel, 1979, 1983; Rockland and Lund, 1982; Gilbert et al., 2000). These intrinsic connections link domains with similar orientation preference, consonant with flank facilitation (Gilbert and Wiesel, 1989; Malach et al., 1993; Weliky et al., 1995; Bosking et al., 1997; Kisvarday et al., 1997; Schmidt et al., 1997). An alternative source of these contextual modulations could be feedback to V1 from higher cortical areas. The experiments described here address these possibilities by comparing the relationships of V1 intrinsic connections and V2 to V1 feedback to the functional architecture of V1.

Quantitatively comparing anatomical pathways requires complete and reproducible axonal labeling. This study uses a new technique to label cortical axons, a recombinant adenovirus bearing the GFP gene, based upon adenovirus's ability to transfer genes to adult primate neurons (Davidson et al., 1993; Akli et al., 1993; Bajocchi et al., 1993). This technique has several advantages over currently used extracellularly injected tracers, including stronger axonal labeling and improved localization of labeled cell somata.

Results

GFP-Labeled Intrinsic Horizontal Axons in V1

A GFP adenovirus was used to label intrinsic connections arising from cells in parts of V1 mapped for orientation and visuotopy (Figure 1A). The virus produces GFP in both glia and neurons. In neurons, GFP fills somata and dendrites in addition to strongly labeling axons (Figure 1B). Labeled cell numbers are controlled by the injection sizes, and the cells are limited to well defined injection sites (Figure 1C). The only existent tracer is that translated in infected cells, and it is absent from the extracellular space, allowing both the unambiguous demarcation of injection sites and counting of labeled cells. Also, because GFP expression always originates in nuclei, all cell bodies with labeled axons can be identified. These somata virtually always lay in the injection sites, indicating that the virus neither labels axons of passage nor acts retrogradely.

Injections in superficial V1 yield dense, continuous labels of horizontally extending axons within 400–500 μm that coalesce into patches beyond that distance (Figures 2A and 2B). The axons were imaged using confocal microscopy, providing high resolution not only within the plane of section, but also in depth. Reconstructions were assembled from multiple z stacks—~50 depth planes into which each cortical slice was optically sectioned—within grids covering the projections, as evident in the tiled appearance of Figure 2A. Axon patches continue across adjacent sections, demonstrating that the intrinsic connections form columns of label throughout the superficial layers (Figures 2C and 2D). The farthest-extending axons produce patches 3.5 mm away from the injections. To relate the axonal patterns to functional maps, the axons were hand-traced from the confocal z stacks (Figure 3A).

Visuotopy of the Intrinsic Horizontal Connections

The visuotopic extents of reconstructed axonal fields were determined by mapping RFs in the vicinities of the injection sites (Figure 4). Cortical locations were assigned visuotopic coordinates by warping interpolated

[3] Correspondence: gilbert@rockefeller.edu

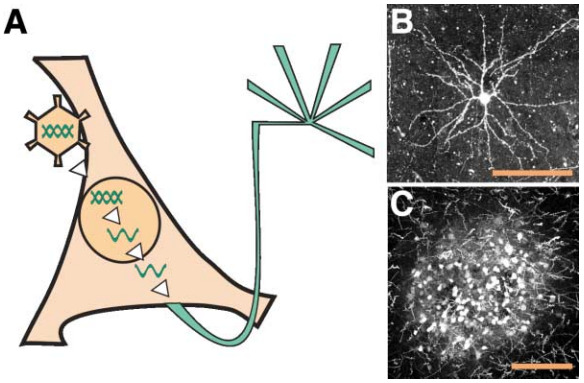

Figure 1. Delivery of GFP Gene to Cortical Neurons by Adenovirus

(A) The technique produces GFP expression only in infected cells and does not introduce label to the extracellular space.

(B) The GFP strongly labels neuronal somata and dendrites.

(C) The number of labeled cells is controlled by the size of the viral injection, and the somata of labeled cells can clearly be discerned and counted.

Scale = 100 μm for (B) and (C).

retinotopic maps based upon these RF locations to the surface of V1. The axonal density of the reconstruction in Figure 3A, plotted in these spatial coordinates, is shown in Figure 4B, with the height of each bar indicating the total integrated axon length within each position in a 10′ × 10′ grid of the visuotopic projection. Labeled axons extend to portions of V1 representing parts of visual space almost 2° away from the injection. Superimposing a 2D rendering of axonal density upon the portion of visual space represented by the labeled region of V1 reveals that this intrinsic projection, stretching nearly 4° end to end, covers an area eight times the linear extent of the minimum response fields for neurons in superficial V1, which average 0.5° in length at this eccentricity (Figure 4C).

Our mapping also allowed us to determine the relation between visuotopy and ocular dominance (OD, Figure 5). As previously observed, the OD columns run anteroposteriorly near the lunate sulcus and orthogonally intersect the V1/V2 border (Figure 5C; LeVay et al., 1975). Close to the V1/V2 border, magnification factor (distance in cortex divided by degrees of visual space) along the mediolateral axis (average = 2.8 mm/°) is larger than that along the anteroposterior axis (average = 1.8 mm/°). The anisotropy of global magnification found between the axes might, therefore, result from the duplication of the retinotopic map by the two sets of ocular dominance columns (Hubel and Wiesel, 1977; Tootell et al., 1988; Blasdel and Campbell, 2001).

Away from the border, swaths of the ocular dominance columns change their axes of orientation. Isoazimuth lines in our visuotopic maps remain nearly orthogonal to the OD columns, even when the columns shift their orientation by 45° relative to the V1/V2 border

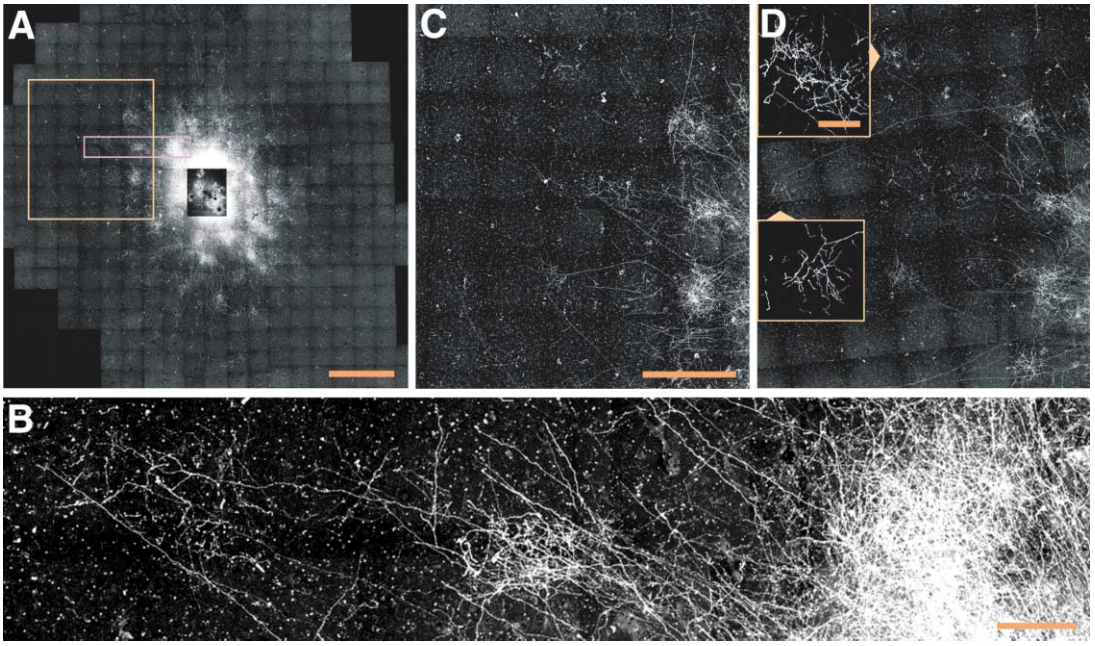

Figure 2. Horizontal Connections Labeled by GFP Adenovirus

(A) The virus yields strong axonal labeling. A 50 μm tangential slice from the superficial layers of V1 lying 300 μm from the cortical surface, imaged at high power through confocal microscopy, shows dense patches of axons surrounding an injection labeling 8800 cells. The injection site is presented with low brightness to indicate the restricted field of labeled somata.

(B) The pink-outlined segment in (A), magnified, exhibits patches at multiple distances from the injection site. Cortical tissue contains punctate background in the emission range of GFP.

(C and D) A closeup of the orange-outlined portion of (A) shows patches that are aligned with those in an adjacent section (D), indicating that the intrinsic axons form columns of connectivity in superficial V1. Insets in (D) contain combined axons from the two sections for distal patches (arrowheads) with the background removed.

Scale = 1 mm for (A), 500 μm for (C) and (D), and 100 μm for (B) and (D) insets.

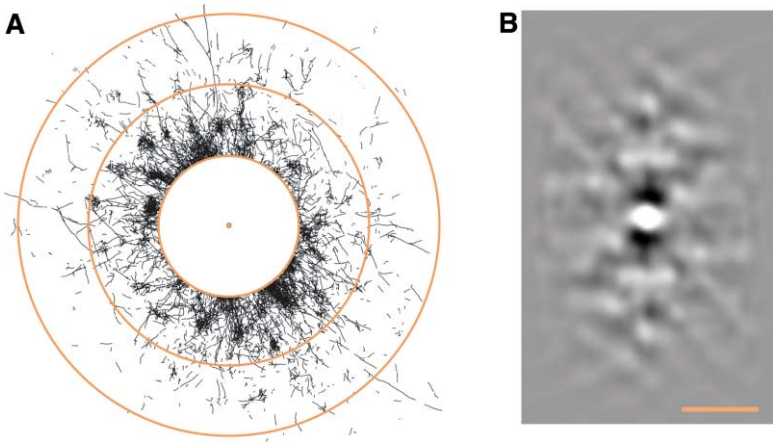

Figure 3. Distribution of Intrinsic Horizontal Connections

(A) Traced axons from a 50 μm section in superficial V1 stretch 7 mm end to end. Axons closer than 1 mm were not traced. The rings are spaced at 1 mm.

(B) Autocorrelation analysis revealed the extent of clustering in the intrinsic connections. An image of a portion of the intrinsic projection was multiplied by itself at various displacements in X and Y, and the products were summed to create a correlogram. The bright center corresponds to absolute correlation when the image is completely aligned with itself, and the surrounding peaks with 0.75 mm spacing indicate clustering of the intrinsic connections with that periodicity.

Scale = 1 mm.

(Figure 5D). This result, found throughout our experiments, is consistent with a similar comparison between the columns and visuotopic map shown earlier (Hubel and Freeman, 1977) and indicates an even finer correspondence between the visuotopic grid and local changes in the direction of OD columns. This finding also corresponds well with a theoretical study of ocular dominance stripe orientation based upon the constraints of binocular disparity processing (Chklovskii, 2000).

Clustering and Orientation Specificity of the Intrinsic Horizontal Connections

Clustering of the intrinsic connections was assessed by autocorrelation (Figure 3B). The correlogram exhibits the expected peak at the center corresponding to multiplication of the axonal map by itself with no shift. Peaks with 0.75 mm spacing are also present and indicate that the axonal distribution has a patchy pattern of 0.75 mm periodicity. The spacing of these patches matches the width of one orientation hypercolumn in V1, suggesting a relationship between the two. This relationship was confirmed when the intrinsic projections from smaller injections, restricted to limited ranges of orientations, were compared with optical imaging orientation maps of the same regions of cortex. For this analysis, intrinsic connections reconstructed from tangential sections were warped, using vertically oriented blood vessels as fiduciary marks, to align precisely with the cortical surface vasculature imaged in vivo. Although the vessels in the tissue slices could be made to line up roughly with the surface vessels viewed in vivo by global warping procedures such as resizing and/or rotation of the entire slices, these manipulations often left discrepancies between the two maps of as much as 400 μm (Figure 6). Such discrepancies are large enough to introduce large errors when comparing the connections with functional architecture.

Results of two experiments in which the warped intrinsic projections were compared with the orientation map directly are shown in Figure 7. In these experiments, the injections were approximately 200 μm in diameter and labeled neurons in columns spanning narrow ranges of orientations (Figures 7D–7F, light bars). The proximal portions of the projections tend to be nonspecific (Figure 7B). At distances beyond 400–500 μm from the injection sites, however, the projections become much more specific for orientation. The orientation distributions of horizontal connections beyond 1 mm diameter circles centered on the injections take the form of bell curves with peaks centered at the same orientations as the injection sites (Figures 7C and 7F) and having bandwidths of roughly 60°. The intrinsic connections therefore show a pattern of like-to-like connections between columns of the same orientation, with some amount of scatter.

Visuotopy and Density of Feedback Connections from V2 to V1

Feedback connections from V2 to the same region of V1 were labeled by injecting the GFP adenovirus into columns of cells (including both superficial and deep layers) in V2 near the lunate sulcus (Figure 8). As previously reported, individual feedback axons rise from the white matter to layer 1 then turn to run parallel to the cortical surface, occasionally sending off collaterals to layer 2 (Rockland and Virga, 1989). The projection is strongest within 100 μm from the cortical surface and, with greater depth, becomes less widespread and less dense (Figure 8C). Figure 9A depicts the feedback projection in superficial V1 from a smaller V2 injection. Both larger and smaller injections produce feedback in V1 stretching 6 mm end to end, comparable to the extent of the intrinsic connections.

A 2D plot depicting the visuotopic extent of feedback resulting from the larger injection indicates that, like the intrinsic connections, V2 feedback extends over an area of cortex representing a wider portion of visual space (approximately 2.5° end to end) than the minimum response fields of superficial layer neurons (Figure 8D). However, comparison of the density of intrinsic and feedback connections, normalizing the figures for labeled cell number, reveals that the intrinsic connections are more than an order of magnitude denser than the feedback (Figure 10).

Lack of Clustering and Orientation Specificity of V2 to V1 Feedback

Unlike the intrinsic connections, which are patchy in every injection, V2 to V1 feedback has different degrees of patchiness in different injections. The feedback with

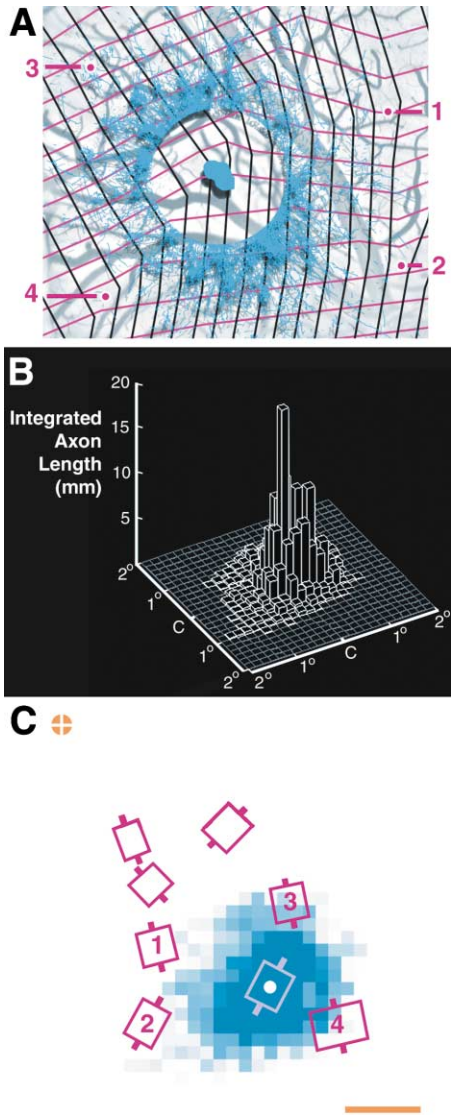

Figure 4. Visuotopic Extent of Intrinsic Horizontal Connections

(A) Local integrated axonal length of the intrinsic connections was assessed as a function of visuotopic location in a 10′ × 10′ grid surrounding the injection site. A portion of the reconstruction shown in Figure 3A is superimposed (in blue) over a picture of the surface vasculature for that part of V1 with recording sites (in purple) corresponding to the RFs shown in (C). A warped, 10′ × 10′ visuotopic grid, computed from the RF positions and assuming smooth and continuous visuotopy, is also shown with iso-elevation lines in purple and iso-azimuth lines in black.

(B) Data presented are from a single 50 μm slice resulting from an injection labeling 8800 cells in superficial V1. Only axons beyond 1 mm from the injection are included, creating a hole in the center of the projection that is obscured by the three-dimensional plot. Axons reach positions in cortex representing portions of visual space nearly 2° away from the center in this region of V1 covering 2°–6° from the fovea.

(C) Superimposing a two-dimensional plot of intrinsic axon density on the map of visual space further illustrates the widespread nature of the connections. Local superficial RF cores average 0.5° in length. Axon density is expressed as shades of blue, darker indicating higher values, with the center filled and values saturated at 0.1 mm per bin to highlight the farthest-reaching axons. The orange circle is the fovea and the scale = 1°.

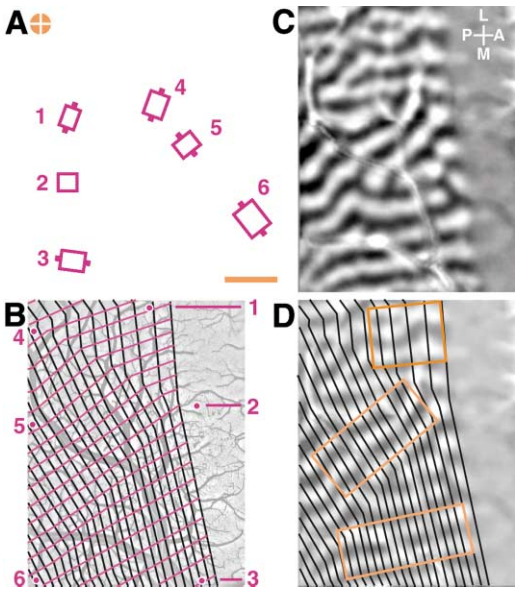

Figure 5. Relation between Visuotopic and Ocular Dominance in V1

(A and B) Superficial RF positions and sizes are presented for sites in V1, marked in (B), lying on the anterior operculum. In (B), the purple lines correspond to iso-elevation (horizontal) contours and black lines correspond to iso-azimuth (vertical) contours, both spaced at 10' intervals, as computed from local RF positions. Across all experiments, the grid elements are generally elongated along the mediolateral axis. In (A), the circle marks the fovea and the scale = 1°.

(C) Optical imaging of ocular dominance columns near the lunate sulcus shows their abrupt cessation at the V1-V2 border.

(D) Superimposition of the interpolated visuotopic maps with the ocular dominance columns indicates that the iso-azimuth contours are roughly orthogonal to the columns, a relationship seen in all experiments.

the most clustering is that resulting from the largest injection (falling in a cytochrome oxidase (CO) dark stripe; Figure 8A). This projection's autocorrelogram exhibits modulation similar in magnitude to that of the intrinsic connections but with a peak-to-peak spacing of 0.5 mm (Figure 8E). The other three fully reconstructed V2 injections, two in CO pale stripes and all targeted to highly orientation-specific domains, do not exhibit this degree of clustering (Figure 9B).

The 0.5 mm periodicity of the feedback with highest clustering suggests that it should not have an iso-orientation relationship with the orientation domains in V1, which cycle at 0.75 mm intervals. This relationship was visualized directly in four experiments with injections in highly oriented sites in V2. Figure 11 shows feedback in V1 from an injection approximately 200 μm in diameter in a pale stripe in V2 (Figure 11F) and restricted to a narrow range of orientations (Figure 11B, gray patch; Figure 11C, light yellow bars). Comparing the distribution of axons with the orientation map shows little specificity in the projection (Figures 11B and 11C, dark yellow bars). A similar lack of orientation specificity is found in the example with the greatest degree of clustering from a CO dark stripe injection (Figure 8 and Figure 12C). Again, the labeled cell bodies are restricted to a limited range of orientation columns (Figure 12A, inset; Figure 12C, light yellow bars), but the orientation distribution

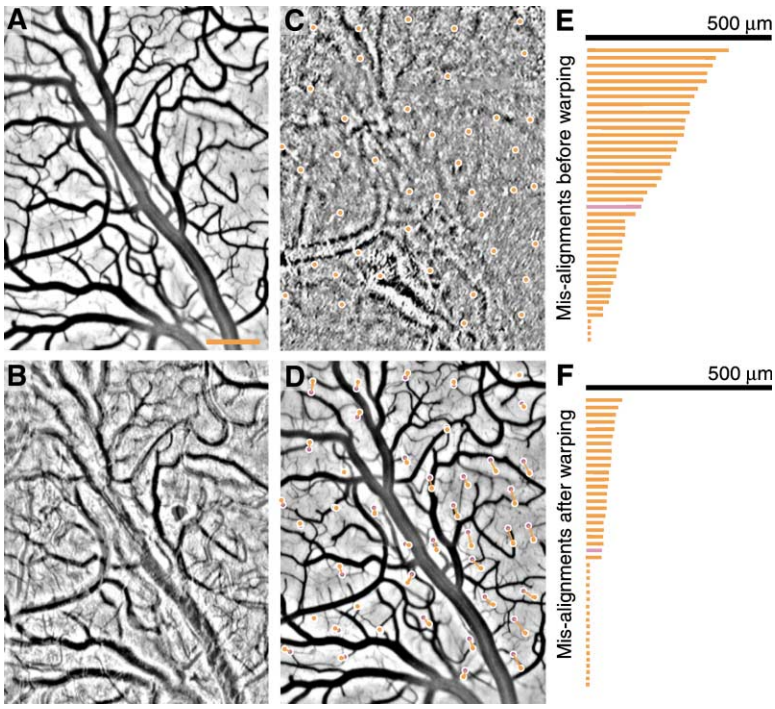

Figure 6. Warping Necessary for Alignment of Functional and Anatomical Maps

(A) During optical imaging of functional domains, the cortical surface vasculature is imaged.

(B) The vascular pattern is also present in slices closest to the pia after the tissue has been processed for anatomy. The uppermost slice is depicted.

(C) Vestiges of the vascular imprint remain deeper in the superficial layers where most of the axonal information is obtained. For these slices, the cross-sections of vertically-oriented blood vessels (marked in orange) can be matched with their correspondents in the optical imaging vascular image to check for alignment between the slice-derived anatomical information and the optical imaging functional maps.

(D) Despite global transformation (such as resizing and rotation) of the slice image to align it with the optical imaging vasculature, local misalignments persist. The positions of vessels in the slice (still in orange) overlap with their representations in the optical image map (in purple) in the upper right and lower left corners of the image but are shifted in the lower right corner.

(E) Without local warping, misalignments between the two maps–compiled from (D) and presented in rank order–can reach 400 μm, with a 140 μm median shift in this example.

(F) After local warping is conducted (with a different set of points from those used for testing) the misalignments are greatly reduced.

Scale = 1 mm in (A)–(D).

of the axonal projection is flat (Figure 12C, dark yellow bars). This nonspecificity of V2 to V1 feedback was found in two additional V2 feedback projections, including a second pale stripe injection (Figure 12D). For all four cases, we split the feedback pattern into a central zone (circle of 500 μm radius) and a distal zone (the complement) and found both zones equally uncorrelated with orientation. In sum, although the V2 injections were re-

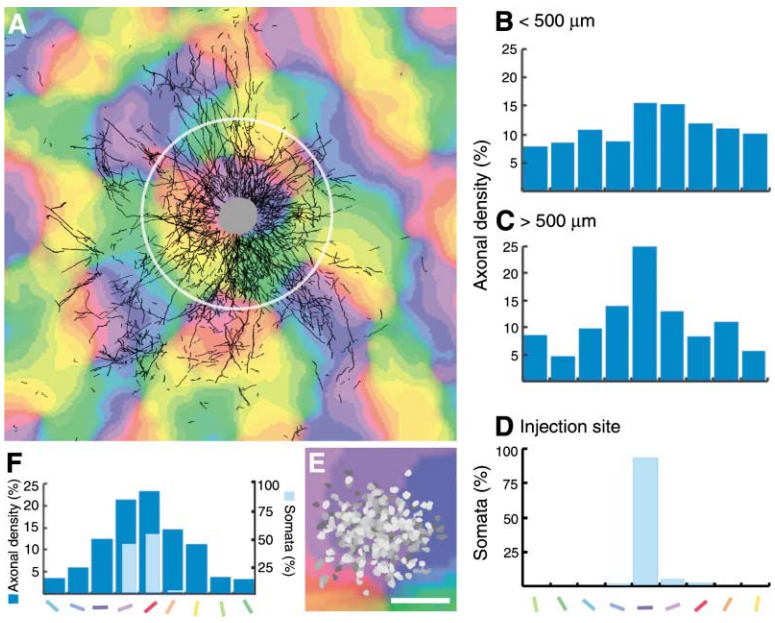

Figure 7. Orientation Specificity of V1 Intrinsic Horizontal Connections

(A–D) Axons from an injection labeling 320 cells in the superficial layers of V1 are superimposed upon the optical imaging orientation map (color-coded as depicted in [D] and [F]) for that portion of cortex. The white ring is 1 mm in diameter. While the axons proximal to the injection site display little orientation specificity (B), patches that form ~500 μm from the injection are targeted to orientation domains of similar preference (C) to their cell bodies (D).

(E) A closeup view of the injection site reveals the spatial distribution of labeled somata relative to the orientation map. Cell bodies are rendered in gradations of gray, with darker shades indicating greater distance from the pia.

(F) Histogram of a second V1 injection labeling 1630 cells with the axonal orientation distribution (>500 μm from the injection) in dark blue and the injection site distribution in light blue. This injection, covering a slightly wider range of orientations than the first, nevertheless yielded a highly orientation-specific projection.

Scale = 100 μm in (E).

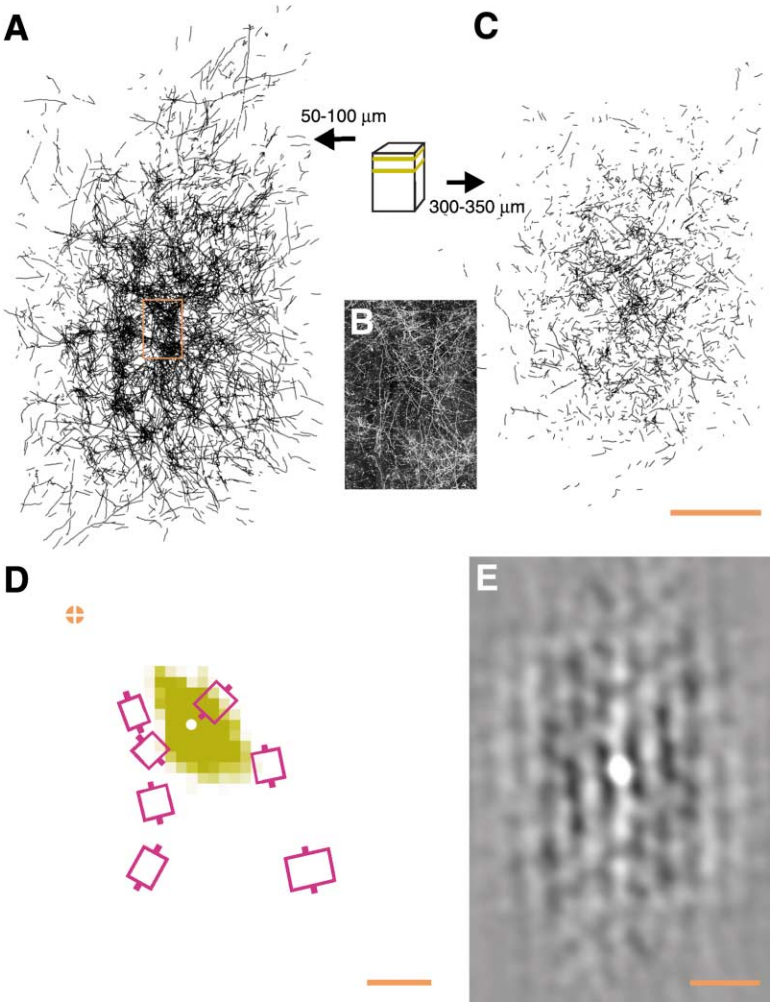

Figure 8. Feedback Projections from V2 to V1

(A) Axons resulting from a V2 injection (labeling 14,600 cells in a column including both superficial and deep layers) stretch 6 mm end to end as traced from a 50 μm horizontal section from layer 1 of V1.

(B) Sample from portion of reconstruction outlined in (A) of the confocal image of feedback.

(C) Traced axons from a 50 μm slice deeper in the superficial layers are less dense than those in layer 1.

(D) A 2D density map of the axonal projection in (A), warped into visuotopic coordinates, is superimposed upon the portion of visual space represented by the part of V1 covered by the axonal field (the values are saturated at 0.1 mm per bin to highlight the farthest-reaching axons, as in Figure 4, for the intrinsic connections).

(E) Autocorrelation analysis of the axonal projection in (A) shows modulation with a 0.5 mm periodicity.

Scale = 1 mm in (C) and (E), and 1° in (D).

stricted to regions representing only limited ranges of orientations, the resulting feedback does not preferentially target domains with similar orientation specificity in V1 but covers all orientation domains evenly.

Discussion

We have determined the cortical and visuotopic extents of V1 intrinsic and V2 to V1 feedback connections. In cortical distance, V1 intrinsic connections stretch 7 mm end to end. The connections from a single locus, therefore, encompass eight to ten full cycles of orientation columns with a 0.75 mm periodicity as highlighted by up to five rings of patches surrounding the injection sites. Visuotopically, the connections cover regions of V1 representing 4° of visual space at 4° eccentricity. V2 to V1 feedback stretches over a comparable distance, but its density is an order of magnitude lower at all points along its distribution. Also, whereas the intrinsic connections preferentially link domains having similar orientation preference, V2 to V1 feedback shows no orientation selectivity.

Recombinant Adenovirus Is a Powerful Axonal Tracer

This analysis was made possible by the development of an adenoviral-mediated method for labeling axons in cortex. Unlike other techniques, the adenoviral method permits the precise comparison of injections through the counting of labeled cells because it does not saturate the extracellular space at the injection site with tracer. Moreover, because the virus's genetic payload must be brought to the infected cell's nucleus before it can be converted into tracer, there is no possibility of labeling axons of passage without seeing labeled cell bodies. In practice, the technique does not label axons of passage and produces no retrograde labeling, making it especially useful for the anterograde quantification of cortical circuitry. Finally, the technique gives high-signal-to noise and complete labeling of the dendritic and axonal arbors of infected cells, thereby revealing long-stretching axons that might have been missed with other less-sensitive tracing techniques.

Perhaps due to the strength of this technique, the length of V1 intrinsic connections demonstrated here is greater than that found in some studies in primates employing extracellular injections of biocytin. These injections showed end to end horizontal extents of the connections under 4 mm (e.g., 2.1 mm, Amir et al., 1993; 3.7 mm, Yoshioka et al, 1996; 3.0 mm in squirrel and owl monkey, Sincich and Blasdel, 2001). In addition to the difference in tracer and species, biocytin may provide incomplete labeling from the smaller injections required to study the columnar specificity of the projec-

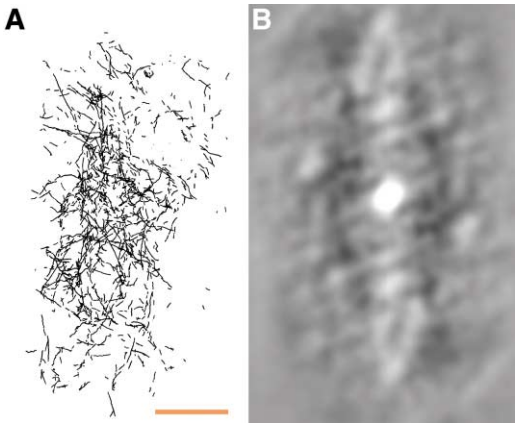

Figure 9. Second Example of V2 to V1 Feedback

(A) Traced feedback from three 50 μm sections, ranging from 50 to 200 μm below the cortical surface, resulting from an injection that labeled 6500 cells. The extent of the projection is ~6 mm.

(B) Its autocorrelogram confirms that the projection has little clustering and contains only low-amplitude and variable periodic variation in density.

Scale = 1 mm for (A) and (B).

tions. Nevertheless, other studies using extracellular injections of biocytin in the cat and tree shrew have shown more extensive axonal arbors, comparable to those reported here (Darian-Smith and Gilbert, 1994; Bosking et al., 1997).

Contextual Interactions in V1 Neuronal Responses

In quantifying the lateral connectivity of superficial V1, these experiments tried to distinguish between mechanisms proposed to underlie contextual interactions contributing to the perceptual assembly of contours. The notion of contextual interactions in V1 relates to how the V1 RF is defined. A common measure of RF size is the minimum response field, where a short line segment is placed at different positions along the orientation axis

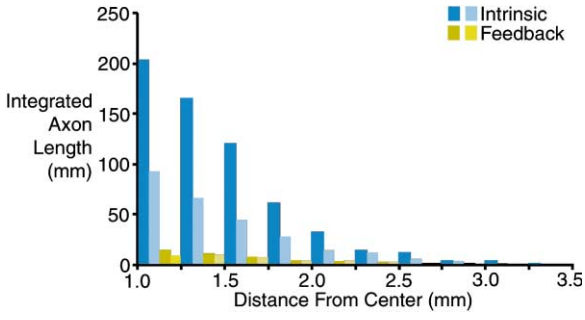

Figure 10. Relative Densities of Intrinsic and Feedback Projections in V1

Axonal length integrated as a function of distance from the injection site for two V1 injections, labeling 13,100 and 8,800 cells in the superficial layers, is shown in dark and light blue, respectively. Feedback resulting from 14,600 and 6,500 cell injections in V2 is shown in dark and light yellow, respectively. The two intrinsic connection values are taken from single slices while the feedback values are the average of two slices, one from layer 1 and one lying deeper in the superficial layers. The values from all injections have been normalized by labeled cell number to that for the 13,100 cell V1 injection.

of the cell and those positions driving a response are designated as falling within the RF. This measure yields RF sizes ~0.5° in length at 4° eccentricity (Ito and Gilbert, 1999; Kapadia et al., 2000). The minimum response field measure of RF size, however, reveals only the tip of an iceberg.

A growing body of work demonstrates that responses to stimuli falling within the minimal response field, the RF core, are modulated by contextual stimuli lying beyond its boundaries. Contextual stimuli do not by themselves activate neurons, but when presented jointly with stimuli within the RF core can facilitate responses several-fold. These findings have led to a change in the definition of the RF, hence the frequently used distinction between the classical and nonclassical RF (Maffei and Fiorentini, 1976; Allman et al., 1985a, 1985b), though even the earliest characterization of the RF recognized modulatory regions beyond the core (Kuffler, 1953). Various manipulations unmask the modulatory regions, including measurements of length tuning at different contrast levels or with test stimuli embedded in complex backgrounds (Kapadia et al., 1999; Sceniak et al., 1999); conditioning with artificial scotomas, which can expand RF size up to 10-fold (Pettet and Gilbert, 1992; Das and Gilbert, 1995a), retinal lesions, which can shift cortical maps by 6–8 mm (Gilbert et al., 1990; Kaas et al., 1990; Heinen and Skavenski, 1991; Gilbert and Wiesel, 1992; Chino et al., 1992; Darian-Smith and Gilbert, 1994, 1995; Das and Gilbert, 1995b); and stimulating with complex figures (Nelson and Frost, 1985; Allman et al. 1985a, 1985b; Gulyas et al., 1987; Orban et al., 1987; Gilbert and Wiesel, 1990; Pettet and Gilbert, 1992; Gilbert and Wiesel, 1992; Kapadia et al., 1995, 1999, 2000; Sillito et al., 1995; Lamme, 1995; Zipser et al., 1996; Toth et al., 1996; Rossi et al., 1996; Levitt and Lund, 1997; MacEvoy et al. 1998; Kinoshita and Komatsu, 2001). The geometry of these contextual interactions in neuronal recordings matches quantitatively with psychophysical measurements of contour saliency (Wertheimer, 1938; Ullman, 1990; Field et al., 1993), perceptual fill-in (Ramachandran and Gregory, 1991), brightness induction (Polat and Sagi, 1993, 1994; Dresp, 1993; Kapadia et al., 1995, 2000), as well as statistical analyses of the geometric properties of natural scenes (Sigman et al., 2001; Geisler et al., 2001). Together, these results support the idea that V1 plays a role in intermediate level vision, mediating processes of contour integration and surface segmentation.

A V1 neuron's response to a complex stimulus cannot be predicted from its responses to simple stimuli. This nonlinear nature of contextual interactions is illustrated by the finding that a flanking line, while not driving a cell's firing when presented alone, can facilitate its response up to 3-fold to a centrally placed stimulus (Kapadia et al., 1995, 2000). Such modulation with flanking stimuli depends on their geometric arrangement, and its strength drops with increased separation along the colinear axis (some facilitation can be seen as far as 2° from the edge of the minimum response field), with offset from colinearity or changes in relative orientation. The nonlinear nature of contextual interactions is paralleled by the physiology of synaptic potentials evoked via the intrinsic connections (Hirsch and Gilbert, 1991). Besides their nonlinear character with respect to stimulus components, contextual interactions in V1 are also dynamic and subject to top-down control, changing with atten-

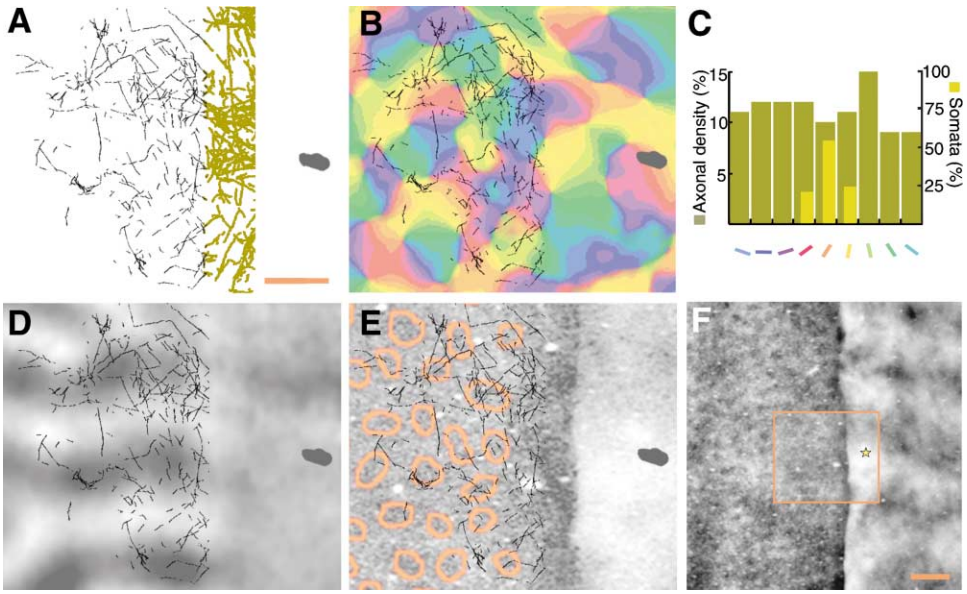

Figure 11. Functional Architecture of V2 to V1 Feedback

(A) Traced axons projecting from a V2 injection labeling 990 cells are relatively sparse and unclustered in V1 (black). The connections within V2 from this injection are shown in yellow. (B) Warping and alignment of the axonal trace with the orientation map shows the orientation selectivity of the injection site in V2 and the lack of orientation specificity of the feedback projection in V1, confirmed by the histogram in (C). Feedback >500 μm from the center of the projection shows no greater orientation specificity than that at the center. The ocular dominance map (D) and a CO stained section (E) delineate the V1/V2 border. The injection falling in a pale stripe near a thick stripe (as indicated by a star in the lower magnification depiction of the stripes in [F] with an orange box outlining the portion shown in closeup in [E]), produces feedback with no ocular dominance or CO specificity in V1 in addition to its lack of orientation specificity. The orange outlines in (E) represent the CO blobs.

Scale = 500 μm in (A) and 1 mm in (F).

tional state, learning, and perceptual task (Ito and Gilbert, 1999; Crist et al., 2001). RF contributions from feedforward pathways such as thalamocortical projections must be distinguished, therefore, from those arising from horizontal and feedback connections, which change according to stimulus properties, context, learning, and higher-order cognitive control.

Long-Range Horizontal Connections Are the Likely Substrate for Contextual Interactions in V1

The results presented here argue that V1 intrinsic, long-range horizontal connections are the source of some of the contextual interactions described above, particularly when compared with V2 to V1 feedback. The clustering of the intrinsic connections, which has a registration with columns of orientation similar to that of the cells of origin, is lacking in V2 to V1 feedback. Intrinsic connection orientation selectivity has been demonstrated by previous studies (Gilbert and Wiesel, 1989; Malach et al., 1993; Weliky et al., 1995; Bosking et al., 1997; Kisvarday et al., 1997; Schmidt et al., 1997). Though the degree of selectivity varies across studies, such variability could result from the local resolution of the warping algorithm as well as differences in selectivity, depending upon distance from the injection shown here and in previous studies (Malach et al., 1993; Bosking et al., 1997). The orientation selectivity of the intrinsic connections is consistent with the orientation dependence of correlated firing, flank facilitation, and contour saliency. Cells in V1 separated by several millimeters show the strongest correlation if they have similar orientation preference (Ts'o et al., 1986). Cellular and perceptual flank facilitation is highly dependent on the orientation of the flanking stimulus and decreases as the flank is rotated from iso-orientation with the central stimulus (Kapadia et al., 1995). In the realm of perceptual saliency, the pop-out character of contours embedded in complex backgrounds is enhanced for contours that are composed of line segments of similar and smoothly changing orientation (Field et al., 1993). The lack of orientation specificity for V2 to V1 feedback makes it unlikely to mediate the contextual interactions involved in contour integration. While it remains to be seen if feedback projections from other areas (e.g., V3, V4, MT) show any relationship with V1 functional architecture, the quantitative approach employed here promises to be a valuable tool in ascertaining their functional significance.

The length of intrinsic horizontal connections, as great as 7 mm end to end in cortical terms and 4° visuotopically, also corresponds well with the scale of contextual interactions seen in psychophysical and physiological investigations of contour integration (Kapadia et al., 1995, 2000; Li and Gilbert, 2002). In humans performing line detection tasks at the same eccentricity as studied in these experiments, the increased ability to detect a target stimulus conferred by a flank persists until the two stimuli are separated by 1.5° to 2.5° (Kapadia et al., 1995). In macaque V1, separations between flanking and

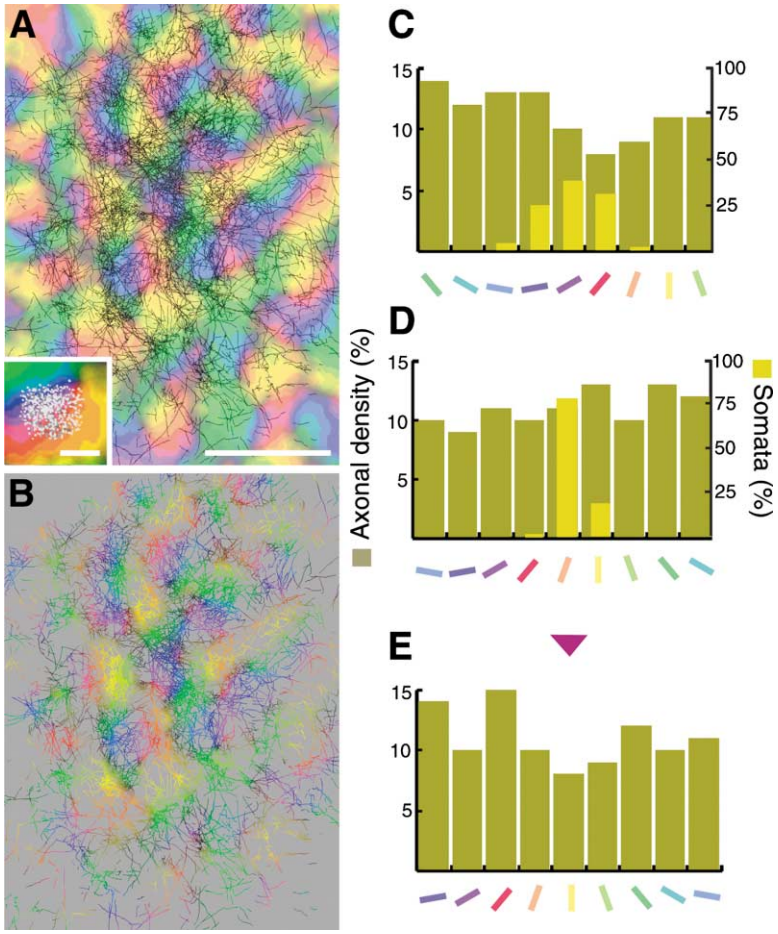

Figure 12. Additional Examples of Orientation Distribution of V2 to V1 Feedback

(A) The traced feedback projection to superficial V1 from another V2 injection (shown in Figure 8) is superimposed upon the orientation map for that portion of cortex. The color code of the map is indicated in the x axis labels of (C)–(E). The injection site in V2, shown as an inset with its traced cells superimposed, covers a restricted range of orientations, but there is no specificity of the feedback connections for orientation domains in V1. Large scale = 1 mm, inset scale = 200 μm.

(B) The same projection presented in (A) is presented again. Only the orientation preferences of the locations where the axons lay are shown; the full range of colors in this image indicates the lack of orientation specificity in the projection.

(C) A histogram showing the orientation preference of the domains in V1 occupied by the feedback projection shown in (A) and (B) (dark yellow) as well as the orientation preference of somata at the injection site (light yellow).

(D) Orientation-specificity histogram for a third feedback projection from V2 to V1, resulting from an injection labeling 1200 cells in a CO pale stripe. The injection, once again, was targeted to a highly orientation-selective site, and labeled cells displayed a very narrow range of orientations, but the feedback projection in V1 exhibited a flat orientation distribution. Color code as in (C).

(E) A fourth injection labeling 6500 cells was made into a site in V2 showing high orientation selectivity as assessed prior to the injection by optical imaging. V2-V1 feedback from the site showed no orientation specificity. The purple triangle marks the orientation of the injection site.

RF center stimuli yield peak cellular response facilitations up to a comparable 2° distance (Kapadia et al., 1995). While most cells show peak facilitation with this stimulus at smaller separations, on average they display some facilitation with flanking stimuli placed up to 2.5° from the RF center (Kapadia et al., 2000). The salience of contours composed of discrete line segments in a complex background breaks down when the gaps between components reach 1.9° to 2.3° (Li and Gilbert, 2002). Interactions serving contour saliency can be augmented in a cascading fashion over a number of nodes in a network of connections, as long as the spacing between elements is kept within this critical distance. In the current study, there is a remarkable consonance between the visuotopic extent of contextual interactions and that of intrinsic horizontal connections. The density of the intrinsic connections also decreases over a 2° center-to-envelope range in a manner consistent with decreasing flank facilitation as the distance is increased between the central RF stimulus and the flank.

Our results indicate that V2 feedback extends over nearly the same distance as the intrinsic connections in superficial V1. Most previous studies examining V2 to V1 feedback have not addressed the extent of the feedback from a single locus in V2 but have verified the topographical nature of the projection (Tigges et al., 1973, 1974; Wong-Riley, 1978, 1979; Rockland and Pandya, 1981; Weller and Kaas, 1983; Symonds and Rosenquist, 1984; Sousa et al., 1991). When the horizontal span of the projection has been reported for primates, however, it has been less than the 6–7 mm end to end extent found here for the macaque (5 mm, Tigges et al., 1981; 5 mm, Perkel et al., 1986; 4.3 mm for a single axon, Rockland and Virga, 1989). As with the intrinsic connections, this discrepancy might result from species differences and the use in previous studies of tracing techniques that did not capture the full scope of the connections. Some have nevertheless concluded, consonant with our own findings, that in cats and primates the projection from a single locus in V2 covers a portion of V1 representing an area of visual space larger than an individual RF (Salin et al., 1989, 1992; Henry et al., 1991; Gattass et al., 1997). Though V2 feedback connections have nearly the same extent as the intrinsic horizontal connections, our technique enabled us to compare their relative densities, revealing that V2 feedback is considerably less dense than the intrinsic connections.

While the character of its distribution suggests that V2 to V1 feedback is not the primary mechanism underlying contextual interactions in V1, it might yet influence such interactions, perhaps by mediating the top-down influences of attention and perceptual task. Recent experiments in humans and monkeys have demonstrated strong attentional modulation of V1 activity, including

an effect upon contour integration (Motter, 1993; Roelfsema et al., 1998; Brefczynski and DeYoe, 1999; Gandhi et al., 1999; Ito and Gilbert, 1999; Martinez et al., 1999; Somers et al., 1999; Crist et al., 2001). This tight relationship between the intrinsic connections mediating the contextual interactions and feedback in turn modulating the intrinsic connections could confound standard physiological approaches to understanding their function. Inactivation of higher cortical areas to isolate the role of the horizontal connections, for instance, will perturb their operation if feedback performs a gating function. Notwithstanding this obstacle to one physiological strategy for elucidating the mechanism, several researchers have tried to determine the source of contextual interactions by examining their time course. Some have found that modulations caused by contextual stimuli begin after a latency which, it is argued, corresponds to the time necessary for feedback to take effect (Lamme, 1995; Zipser et al., 1996; Lamme et al., 1998, 1999; Lee et al., 1998). The relationship between latency and source of input, however, remains unclear, and other researchers have found that feedback acts early in V1 neuronal responses (Hupe et al., 2001). In any event, the contextual modulations most pertinent to contour integration in V1 occur from the beginning of the response (Kapadia et al., 1995, 1999; Ito and Gilbert, 1999). The limitations of physiological attempts to uncover the mechanism of contextual interactions in V1 make quantitative anatomical investigations directed at V1 cortical circuitry such as that reported here valuable for elucidating the role of components of cortical circuits in complex visual functions.

Experimental Procedures

Placement of Tracer Injections

Experiments were performed in three *Macaca fascicularis* and one *Macaca mulatta*. Physiological recordings and tracer injections were made under sterile conditions and with anesthesia in accordance with institutional guidelines for the treatment of primates. All injections were within 15 mm of the midline, the V1 injections < 10 mm and V2 injections < 4 mm from the V1/V2 border. As demonstrated by visuotopic mapping, these regions of V1 and V2 represent the lower half of the visual hemifield near the vertical meridian and between 2° and 6° from the fovea.

Injection Volume and Functional Mapping

The tracer was a recombinant, nonreplicative adenovirus bearing the gene for enhanced GFP with a cytomegalovirus promoter. 20–80 nL (containing 1–4 $\times$ 10^8 virus particles) were pressure injected into optically identified orientation columns in V1 or V2. Minimum response field sizes and positions were mapped using single-cell electrode recording. Ocular dominance and orientation maps were optically measured using intrinsic signals as described previously for the cat but with shutters to segregate stimulation of the two eyes (Das and Gilbert, 1997). Postinjection survival ranged from 6 to 10 days, after which the animals were killed with sodium pentothal and perfused with 4% paraformaldehyde in PBS.

Tissue Processing

After perfusion, the portion of cortex containing the injections was blocked and flattened between two microscope slides. The tissue was then postfixed in paraformaldehyde and subsequently cryoprotected in 30% sucrose. Sections of 30 or 50 μm thickness were mounted in PBS and Gelmount. All samples were stored in the dark at 5°C until analysis. For tissue containing V2 injections, CO staining was performed according to standard procedures.

Confocal Microscope Documentation of GFP-Labeled Axons and Somata

GFP labeling was documented using confocal microscopy (Zeiss LSM). Superficial layer slices 50 to 500 μm deep were imaged at 40× under conditions that varied, depending upon the amount of labeling and prevalence of background autofluorescence. For each sample, the tissue slice was blanketed with z stacks covering the entire region containing GFP-labeled processes either by hand or by using a motorized xy-stage and associated software. For quantitative analysis, the processes were hand-traced from the digital representation, and labeled cell bodies were traced in selected slices for alignment with functional maps and counted throughout the entire depth of the injections using the optical fractionator method of unbiased stereology (West et al., 1991) with StereoInvestigator software (Microbrightfield, Williston, VT). We counted all labeled cell bodies and made no distinction between glia and neurons.

Correlation of Anatomy with Function

Correlation of the anatomical information and physiological data was performed by aligning digital reconstructions of the axons with pictures of the cortical surface vasculature taken at the time of the injections. Axonal reconstructions from the processed tissue were warped and aligned with each other and with the surface vasculature by matching the cross-sections of vertically oriented vessels. The retinotopic extents of the reconstructed axons were obtained by superimposing retinotopic maps interpolated from RF centers corresponding to six to eight electrode recordings for each hemisphere on the cortical surface with the aligned reconstructions. The measurement of axonal density as a function of retinotopic position or orientation preference within the cortex was performed by a program written in the lab using the interactive data language (IDL).

Acknowledgments

We thank Joel Lopez for technical support. We are also grateful to Kara Pham for guidance in stereological procedures and Radha Rangarajan and Alison North for help with the confocal microscope. This work was supported by NIH grants NEI EY07968 and 5T32 GM07524.

Received: January 7, 2002
Revised: September 25, 2002

References

Akli, S., Caillaud, C., Vigne, E., Stratford-Perricaudet, L.D., Poenaru, L., Perricaudet, M., Kahn, A., and Peschanski, M.R. (1993). Transfer of a foreign gene into the brain using adenovirus vectors. Nat. Genet. *3*, 224–228.

Allman, J., Miezin, F., and McGuinness, E. (1985a). Direction- and velocity-specific responses from beyond the classical receptive field in the middle temporal visual area (MT). Perception *14*, 105–126.

Allman, J., Miezin, F., and McGuinness, E. (1985b). Stimulus specific responses from beyond the classical receptive field–neurophysiological mechanisms for local global comparisons in visual neurons. Annu. Rev. Neurosci. *8*, 407–430.

Amir, Y., Harel, M., and Malach, R. (1993). Cortical hierarchy reflected in the organization of intrinsic connections in macaque monkey visual cortex. J. Comp. Neurol. *334*, 19–46.

Bajocchi, G., Feldman, S.H., Crystal, R.G., and Mastrangeli, A. (1993). Direct in vivo gene transfer to ependymal cells in the central nervous system using recombinant adenovirus vectors. Nat. Genet. *3*, 229–234.

Blasdel, G., and Campbell, D. (2001). Functional retinotopy of monkey visual cortex. J. Neurosci. *21*, 8286–8301.

Bosking, W.H., Zhang, Y., Schofield, B., and Fitzpatrick, D. (1997). Orientation selectivity and arrangement of horizontal connections in tree shrew striate cortex. J. Neurosci. *17*, 2112–2127.

Brefczynski, J.A., and DeYoe, E.A. (1999). A physiological correlate of the 'spotlight' of visual attention. Nat. Neurosci. *2*, 370–374.

Chino, Y.M., Kaas, J.H., Smith, E.L., 3rd, Langston, A.L., and Cheng,

H. (1992). Rapid reorganization of cortical maps in adult cats following restricted deafferentiation in retina. Vision Res. *32*, 789–796.

Chklovskii, D.B. (2000). Binocular disparity can explain the orientation of ocular dominance stripes in primate primary visual area (V1). Vision Res. *40*, 1765–1773.

Crist, R.E., Li, W., and Gilbert, C.D. (2001). Learning to see: experience and attention in primary visual cortex. Nat. Neurosci. *4*, 519–525.

Darian-Smith, C., and Gilbert, C.D. (1994). Axonal sprouting accompanies functional reorganization in adult cat striate cortex. Nature *368*, 737–740.

Darian-Smith, C., and Gilbert, C.D. (1995). Topographic reorganization in the striate cortex of the adult cat and monkey is cortically mediated. J. Neurosci. *15*, 1631–1647.

Das, A., and Gilbert, C.D. (1995a). Receptive field expansion in adult visual cortex is linked to dynamic changes in strength of cortical connections. J. Neurophysiol. *74*, 779–792.

Das, A., and Gilbert, C.D. (1995b). Long-range horizontal connections and their role in cortical reorganization revealed by optical recording of cat primary visual cortex. Nature *375*, 780–784.

Das, A., and Gilbert, C.D. (1997). Distortions of visuotopic map match orientation singularities in primary visual cortex. Nature *317*, 58–61.

Davidson, B.L., Allen, E.D., Kozarsky, K.F., Wilson, J.M., and Roessler, B.J. (1993). A model system for in vivo gene transfer into the central nervous system using an adenoviral vector. Nat. Genet. *3*, 219–223.

Dresp, B. (1993). Bright lines and edges facilitate the detection of small line targets. Spat. Vis. *7*, 213–225.

Field, D.J., Hayes, A., and Hess, R.F. (1993). Contour integration by the human visual system: evidence for a local "association field". Vision Res. *33*, 173–193.

Gandhi, S.P., Heeger, D.J., and Boynton, G.M. (1999). Spatial attention affects brain activity in human primary visual cortex. Proc. Natl. Acad. Sci. USA *96*, 3314–3319.

Gattass, R., Sousa, A.P.B., Mishkin, M., and Ungerleider, L.G. (1997). Cortical projections of area V2 in the macaque. Cereb. Cortex *7*, 110–129.

Geisler, W.S., Perry, J.S., Super, B.J., and Gallogly, D.P. (2001). Edge co-occurrence in natural images predicts contour grouping performance. Vision Res. *41*, 711–724.

Gilbert, C.D., and Wiesel, T.N. (1979). Morphology and intracortical projections of functionally characterized neurones in the cat visual cortex. Nature *280*, 120–125.

Gilbert, C.D., and Wiesel, T.N. (1983). Clustered intrinsic connections in cat visual cortex. J. Neurosci. *3*, 1116–1133.

Gilbert, C.D., and Wiesel, T.N. (1989). Columnar specificity of intrinsic horizontal and corticocortical connections in cat visual cortex. J. Neurosci. *9*, 2432–2442.

Gilbert, C.D., and Wiesel, T.N. (1990). The influence of contextual stimuli on the orientation selectivity of cells in primary visual cortex of the cat. Vision Res. *30*, 1689–1701.

Gilbert, C.D., and Wiesel, T.N. (1992). Receptive field dynamics in adult primary visual cortex. Nature *356*, 150–152.

Gilbert, C.D., Hirsch, J.A., and Wiesel, T.N. (1990). Lateral interactions in visual cortex. Cold Spring Harb. Symp. Quant. Biol. *55*, 663–677.

Gilbert, C.D., Ito, M., Kapadia, M.K., and Westheimer, G. (2000). Interactions between attention, context and learning in primary visual cortex. Vision Res. *40*, 1217–1226.

Gulyas, B., Orban, G.A., Duysens, J., and Maes, H. (1987). The suppressive influence of moving textured backgrounds on responses of cat striate neurons to moving bars. J. Neurophysiol. *57*, 1767–1791.

Heinen, S.J., and Skavenski, A.A. (1991). Recovery of visual responses in foveal V1 neurons following bilateral foveal lesions in adult monkey. Exp. Brain Res. *83*, 670–674.

Henry, G.H., Salin, P.A., and Bullier, J. (1991). Projections from area 18 and 19 to cat striate cortex: divergence and laminar specificity. Eur. J. Neurosci. *3*, 186–200.

Hirsch, J.A., and Gilbert, C.D. (1991). Synaptic physiology of horizontal connections in the cat's visual cortex. J. Neurosci. *11*, 1800–1809.

Hubel, D.H., and Freeman, D.C. (1977). Projection into the visual field of ocular dominance columns in macaque monkey. Brain Res. *122*, 336–343.

Hubel, D.H., and Wiesel, T.N. (1977). Functional architecture of macaque monkey visual cortex. Proc. R. Soc. Lond. B Biol. Sci. *198*, 1–59.

Hupe, J.-M., James, A.C., Girard, P., Lomber, S.G., Payne, B.R., and Bullier, J. (2001). Feedback connections act on the early part of the responses in monkey visual cortex. J. Neurophysiol. *85*, 134–145.

Ito, M., and Gilbert, C.D. (1999). Attention modulates contextual influences in the primary visual cortex of alert monkeys. Neuron *22*, 593–604.

Kaas, J.H., Krubitzer, L.A., Chino, Y.M., Langston, A.L., Polley, E.H., and Blair, N. (1990). Reorganization of retinotopic cortical maps in adult mammals after lesions of the retina. Science *248*, 229–231.

Kapadia, M.K., Ito, M., Gilbert, C.D., and Westheimer, G. (1995). Improvement in visual sensitivity by changes in local context: parallel studies in human observers and in V1 of alert monkeys. Neuron *15*, 843–856.

Kapadia, M.K., Westheimer, G., and Gilbert, C.D. (1999). Dynamics of spatial summation in primary visual cortex of alert monkeys. Proc. Natl. Acad. Sci. USA *96*, 12073–12078.

Kapadia, M.K., Westheimer, G., and Gilbert, C.D. (2000). Spatial distribution of contextual interactions in primary visual cortex and in visual perception. J. Neurophysiol. *84*, 2048–2062.

Kinoshita, M., and Komatsu, H. (2001). Neural representation of the luminance and brightness of a uniform surface in the macaque primary visual cortex. J. Neurophysiol. *86*, 2559–2570.

Kisvarday, Z.F., Toth, E., Rausch, M., and Eysel, U.T. (1997). Orientation-specific relationship between populations of excitatory and inhibitory lateral connections in the visual cortex of the cat. Cereb. Cortex *7*, 605–618.

Kuffler, S.W. (1953). Discharge patterns and functional organization of mammalian retina. J. Neurophysiol. *16*, 37–68.

Lamme, V.A., Zipser, K., and Spekreijse, H. (1998). Figure-ground activity in primary visual cortex is suppressed by anesthesia. Proc. Natl. Acad. Sci. USA *95*, 3263–3268.

Lamme, V.A., Rodriguez-Rodriguez, V., and Spekreijse, H. (1999). Separate processing dynamics for texture elements, boundaries and surfaces in primary visual cortex of the macaque monkey. Cereb. Cortex *9*, 406–413.

Lamme, V.A.F. (1995). The neurophysiology of figure-ground segregation in primary visual cortex. J. Neurosci. *15*, 1605–1615.

Lee, T.S., Mumford, D., Romero, R., and Lamme, V.A. (1998). The role of the primary visual cortex in higher level vision. Vision Res. *38*, 2429–2454.

LeVay, S., Hubel, D.H., and Wiesel, T.N. (1975). The pattern of ocular dominance columns in macaque visual cortex revealed by a reduced silver stain. J. Comp. Neurol. *159*, 559–576.

Levitt, J.B., and Lund, J.S. (1997). Contrast dependence of contextual effects in primate visual cortex. Nature *387*, 73–76.

Li, W., and Gilbert, C.D. (2002). Global contour saliency and local colinear interactions. J. Neurophysiol., in press.

MacEvoy, S.P., Kim, W., and Paradiso, M.A. (1998). Integration of surface information in primary visual cortex. Nat. Neurosci. *1*, 616–620.

Maffei, L., and Fiorentini, A. (1976). The unresponsive regions of visual cortical receptive fields. Vision Res. *16*, 1131–1139.

Malach, R., Amir, Y., Harel, M., and Grinvald, A. (1993). Relationship between intrinsic connections and functional architecture revealed by optical imaging and in vivo targeted biocytin injections in primate striate cortex. Proc. Natl. Acad. Sci. USA *90*, 10469–10473.

Martinez, A., Anllo-Vento, L., Sereno, M.I., Frank, L.R., Buxton, R.B., Dubowitz, D.J., Wong, E.C., Hinrichs, N., Heinze, H.J., and Hillyard,

S.A. (1999). Involvement of striate and extrastriate visual cortical areas in spatial attention. Nat. Neurosci. *2*, 364–369.

Motter, B.C. (1993). Focal attention produces spatially selective processing in visual cortical areas V1, V2, and V4 in the presence of competing stimuli. J. Neurophysiol. *70*, 909–919.

Nelson, J.I., and Frost, B. (1985). Intracortical facilitation among co-oriented, co-axially aligned simple cells in cat striate neurons. Exp. Brain Res. *6*, 54–61.

Orban, G.A., Guylas, B., and Vogels, R. (1987). Influence of a moving textural background on direction selectivity of cat striate neurons. J. Neurophysiol. *57*, 1767–1791.

Perkel, D.J., Bullier, J., and Kennedy, H. (1986). Topography of the afferent connectivity of area 17 in the macaque monkey: a double-labeling study. J. Comp. Neurol. *253*, 374–402.

Pettet, M.W., and Gilbert, C.D. (1992). Dynamic changes in receptive-field size in cat primary visual cortex. Proc. Natl. Acad. Sci. USA *89*, 8366–8370.

Polat, U., and Sagi, D. (1993). Lateral interactions between spatial channels: suppression and facilitation revealed by lateral masking experiments. Vision Res. *33*, 993–999.

Polat, U., and Sagi, D. (1994). The architecture of perceptual spatial interactions. Vision Res. *34*, 73–78.

Ramachandran, V.S., and Gregory, R.L. (1991). Perceptual filling-in of artificially induced scotomas in human vision. Nature *350*, 699–702.

Rockland, K.S., and Lund, J.S. (1982). Widespread periodic intrinsic connections in the tree shrew visual cortex. Science *215*, 1532–1534.

Rockland, K.S., and Pandya, D.N. (1981). Cortical connections of the occipital lobe in the rhesus monkey: interconnections between areas *17*, 18, *19*, and the superior temporal sulcus. Brain Res. *212*, 249–270.

Rockland, K.S., and Virga, A. (1989). Terminal arbors of individual "feedback" axons projecting from area V2 to V1 in the macaque monkey: a study using immunohistochemistry of anterogradely transported *Phaseolus vulgaris*-leucoagglutinin. J. Comp. Neurol. *285*, 54–72.

Roelfsema, P.R., Lamme, V.A.F., and Sprekreijse, H. (1998). Object-based attention in the primary visual cortex of the macaque monkey. Nature *395*, 376–381.

Rossi, A.F., Rittenhouse, C.D., and Paradiso, M.A. (1996). The representation of brightness in primary visual cortex. Science *273*, 1391–1398.

Salin, P.A., Bullier, J., and Kennedy, H. (1989). Convergence and divergence in the afferent projections to cat area 17. J. Comp. Neurol. *283*, 486–512.

Salin, P.A., Girard, P., Kennedy, H., and Bullier, J. (1992). Visuotopic organization of corticocortical connections in the visual system of the cat. J. Comp. Neurol. *320*, 415–434.

Sceniak, M.P., Ringach, D.L., Hawken, M.J., and Shapley, R. (1999). Contrast's effect on spatial summation by macaque V1 neurons. Nat. Neurosci. *2*, 733–739.

Schmidt, K.E., Kim, D.-S., Singer, W., Bonhoeffer, T., and Lowel, S. (1997). Functional specificity of long-range intrinsic and interhemispheric connections in the visual cortex of strabismic cats. J. Neurosci. *17*, 5480–5492.

Sigman, M., Cecchi, G.A., Gilbert, C.D., and Magnasco, M.O. (2001). On a common circle: natural scenes and Gestalt rules. Proc. Natl. Acad. Sci. USA *98*, 1935–1940.

Sillito, A.M., Grieve, K.L., Jones, H.E., Cudeiro, J., and Davis, J. (1995). Visual cortical mechanisms detecting focal orientation discontinuities. Nature *378*, 492–496.

Sincich, L.C., and Blasdel, G.G. (2001). Oriented axon projections in primary visual cortex of the monkey. J. Neurosci. *21*, 4416–4426.

Somers, D.C., Dale, A.M., Seiffert, A.E., and Tootell, R.B.H. (1999). Functional MRI reveals spatially specific attentional modulation in human primary visual cortex. Proc. Natl. Acad. Sci. USA *96*, 1663–1668.

Sousa, A.P.B., Pinon, M.C., Gattass, R., and Rosa, M.G.P. (1991). Topographic organization of cortical input to striate cortex in the *Cebus* monkey: a fluorescent tracer study. J. Comp. Neurol. *308*, 665–682.

Symonds, L.L., and Rosenquist, A.C. (1984). Corticocortical connections among visual areas in the cat. J. Comp. Neurol. *229*, 1–38.

Tigges, J., Spatz, W.B., and Tigges, M. (1973). Reciprocal point-to-point connections between parastriate and striate cortex in the squirrel monkey. J. Comp. Neurol. *148*, 481–490.

Tigges, J., Spatz, W.B., and Tigges, M. (1974). Efferent cortico-cortical fiber connections of area 18 in the squirrel monkey (*Saimiri*). J. Comp. Neurol. *158*, 219–236.

Tigges, J., Tigges, M., Anschel, S., Cross, N.A., Letbetter, D., and McBride, R.L. (1981). Areal and laminar distribution of neurons interconnecting the central visual cortical areas 17, 18, 19, and MT in squirrel monkey (*Saimiri*). J. Comp. Neurol. *202*, 539–560.

Tootell, R.B.H., Switkes, E., Silverman, M.S., and Hamilton, S.L. (1988). Functional anatomy of macaque striate cortex. II. Retinotopic organization. J. Neurosci. *8*, 1531–1568.

Toth, L.J., Rao, S.C., Kim, D.-S., Somers, D., and Sur, M. (1996). Subthreshold facilitation and suppression in primary visual cortex revealed by intrinsic signal imaging. Proc. Natl. Acad. Sci. USA *93*, 9869–9874.

Ts'o, D.Y., Gilbert, C.D., and Wiesel, T.N. (1986). Relationships between horizontal interactions and functional architecture in cat striate cortex as revealed by cross-correlation analysis. J. Neurosci. *6*, 1160–1170.

Ullman, S. (1990). 3-dimensional object recognition. Cold Spring Harb. Symp. Quant. Biol. *55*, 889–898.

Weliky, M., Kandler, K., Fitzpatrick, D., and Katz, L. (1995). Patterns of excitation and inhibition evoked by horizontal connections in visual cortex share a common relationship to orientation columns. Neuron *15*, 541–552.

Weller, R.E., and Kaas, J.H. (1983). Retinotopic patterns of connections of area 17 with visual areas V-II and MT in macaque monkeys. J. Comp. Neurol. *220*, 253–279.

Wertheimer, G. (1938). Laws of Organization in Perceptual Forms. (London: Harcourt, Brace and Jovanovich).

West, M.J., Slomianka, L., and Gundersen, H.J. (1991). Unbiased stereological estimation of the total number of neurons in the subdivisions of the rat hippocampus using the optical fractionator. Anat. Rec. *231*, 482–497.

Wong-Riley, M. (1978). Reciprocal connections between striate and prestriate cortex in squirrel monkey as demonstrated by combined peroxidase histochemistry and autoradiography. Brain Res. *147*, 159–164.

Wong-Riley, M. (1979). Columnar cortico-cortical interconnections within the visual system of the squirrel and macaque monkeys. Brain Res. *162*, 201–217.

Yoshioka, T., Blasdel, G.G., Levitt, J.B., and Lund, J.S. (1996). Relation between patterns of intrinsic lateral connectivity, ocular dominance, and cytochrome oxidase-reactive regions in macaque monkey striate cortex. Cereb. Cortex *6*, 297–310.

Zipser, K., Lamme, V.A.F., and Schiller, P.H. (1996). Contextual modulation in primary visual cortex. J. Neurosci. *16*, 7376–7389.